# Nanoscale Stabilization of Sodium Oxides: Implications for Na–O$_2$ Batteries

ShinYoung Kang, Yifei Mo, Shyue Ping Ong, and Gerbrand Ceder*

Department of Materials Science and Engineering, Massachusetts Institute of Technology, Cambridge, Massachusetts 02139, United States

**Ⓢ** *Supporting Information*

**ABSTRACT:** The thermodynamic stability of materials can depend on particle size due to the competition between surface and bulk energy. In this Letter, we show that, while sodium peroxide (Na$_2$O$_2$) is the stable bulk phase of Na in an oxygen environment at standard conditions, sodium superoxide (NaO$_2$) is considerably more stable at the nanoscale. As a consequence, the superoxide requires a much lower nucleation energy than the peroxide, explaining why it can be observed as the discharge product in some Na–O$_2$ batteries. As the superoxide can be recharged (decomposed) at much lower overpotentials than the peroxide, these findings are important to create highly reversible Na–O$_2$ batteries. We derive the specific electrochemical conditions to nucleate and retain Na-superoxides and comment on the importance of considering the nanophase thermodynamics when optimizing an electrochemical system.

**KEYWORDS:** *Size-dependent stability, Na–air batteries, NaO$_2$, Na$_2$O$_2$, sodium superoxide, sodium peroxide*
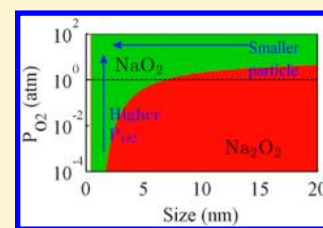
It is known that the particle size dependent stability of polymorphs can influence their nucleation, growth, and phase transformation.[1–5] In this paper we investigate the size, temperature, and $P_{O_2}$ dependence of the phase stability of sodium oxides and the role that this phase selection at the nanoscale plays in the operation of Na–O$_2$ batteries. Besides the recent interest in sodium oxides for batteries with high specific energy, these oxides are important as they have broad applications in glasses (Na$_2$O) and as oxidizing agents (Na$_2$O$_2$). Recently, the relative stability of Na–O compounds has drawn attention in the battery community as the performance of Na–O$_2$ batteries depends strongly on which particular oxide is formed as the discharge product.[6–14]

Although the discharge products of Na–O$_2$ batteries have a somewhat lower theoretical specific energy (1.6 kWh/kg when Na$_2$O$_2$ is formed, and 1.1 kWh/kg when NaO$_2$ is formed) than that in Li–O$_2$ batteries (3.5 kWh/kg when Li$_2$O$_2$ is formed), the chemical difference between the two alkali metals differentiates the properties of Na–O$_2$ and Li–O$_2$ electrochemistry in a substantial way. In the Na–O system, NaO$_2$ as well as Na$_2$O$_2$ are stable compounds, while in the Li–O system LiO$_2$ is not a stable compound at standard state conditions (300 K and 1 atm).[15,16] The phase stability of the metal superoxide is significant, because when the superoxide ion goes in solution, it is very reactive against solvent molecules and carbon support.[17–19] Preventing the electrolyte reactivity with the superoxide ions is one of the hardest challenges in Li–O$_2$ batteries. On the other hand, because a stable state of NaO$_2$ is accessible, the superoxide ions can react with Na ions to form solid NaO$_2$ in a Na–O$_2$ battery, as was observed by Hartmann et al.[13,14]

However, there are remaining questions in Na–O$_2$ electrochemistry—some studies[13,14] reported NaO$_2$ as the main discharge product, while others[6–12] reported Na$_2$O$_2$. When Na$_2$O$_2$ is formed as a discharge product the cells show poor reversibility (<10 cycles) and high overpotentials (from 0.3 V to higher than 1.0 V),[6–11] similar to the problems when recharging Li–O$_2$ cells. On the other hand, the charge and discharge overpotentials are reduced to less than 200 mV when NaO$_2$ forms,[13,14] offering prospects for highly reversible Na–O$_2$ batteries. Currently, there is no understanding of how reaction conditions control the formation of either peroxide or superoxide.

In this work, we investigate the thermodynamic stability of Na–O compounds as a function of temperature, O$_2$ partial pressure, and particle size using first-principles calculations. We calculate the energy of bulk Na–O compounds, and combine them with environmentally equilibrated surface energies, to construct phase diagrams as function of particle size and O$_2$ partial pressure. Using this thermodynamic information in a nucleation model, we find that the superoxide NaO$_2$ is the preferred nanoparticle product at large $P_{O_2}$ or at small discharge overpotential, indicating that it is the most likely phase to nucleate first, even when Na$_2$O$_2$ is the thermodynamically preferred bulk state. Hence, our results show that understanding the particle-size dependence of phase stability is crucial for understanding nucleation.

We considered all Na–O compounds and polymorphs reported by Wriedt:[15] Na$_2$O, Na$_2$O$_2$, NaO$_2$, and NaO$_3$.[20,21] The structures of these compounds are displayed in Figure 1. The stable structure of NaO$_2$ below 196 K has the *Pnnm* space group, which is shown in Figure 1d. Between 196 and 223 K,
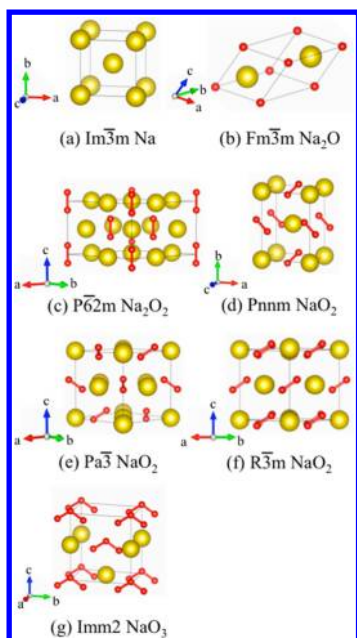
**Figure 1.** Structures of (a) $Im\bar{3}m$ Na metal, (b) $Fm\bar{3}m$ Na$_2$O, (c) $P\bar{6}2m$ Na$_2$O$_2$, NaO$_2$ polymorphs; (d) $Pnnm$, (e) $Pa\bar{3}$ (ordered form of $Fm\bar{3}m$), and (f) $R\bar{3}m$, and (g) $Imm2$ NaO$_3$. Yellow spheres are Na ions, and red spheres are O ions with their bonds marked as red bars.

the $Pa\bar{3}$ structure is the stable form of NaO$_2$. This structure is derived from the NaCl rocksalt structure with O$_2$ dimers centered on the "Cl" lattice positions and aligned along the $\langle 111 \rangle$ directions as shown in Figure 1e. Above 223 K, O$_2$ bonds freely rotate, leading to the $Fm\bar{3}m$ space group.[20,21] More information on these compounds can be found in the Supporting Information (SI).

We performed total energy calculations using the Vienna ab initio simulation package (VASP)[22] and the projector augmented-wave (PAW) approach[23] within the generalized gradient approximation (GGA) to density functional theory (DFT). We calculated the ground state energies of O$_2$ gas and the Na−O compounds in Figure 1. For Na, the 2p and 3s states were treated as valence states using an Na_pv ($2p^6\ 3s^1$) pseudopotential. The O ($2s^2\ 2p^4$) pseudopotential was used for oxygen. The energy cutoff for plane-waves was set to 520 eV, and the energies and forces were converged within $10^{-6}$ eV and $10^{-3}$ eV/Å per formula unit, respectively. The spacing of the $\Gamma$-centered $k$-point meshes was set to less than 0.05 Å$^{-1}$. It is known that standard semilocal DFT significantly overbinds the O$_2$ molecule, which in turn leads to large errors in the calculated formation energies of oxides (O$^{2-}$), peroxides (O$_2^{2-}$) and superoxides (O$_2^{-}$), due to the different degrees in which the O═O double bond is broken in these systems and the different number of electrons transferred.[24−26] To make the comparison of the relative stability of Na−O compounds more accurate, we calculated and applied an oxidation energy correction $E_{oxd}$ in the spirit of Wang et al.[27] The correction is different for oxides, peroxides, and superoxides; we believe this is a more accurate reflection of the underlying physical limitations of DFT, as compared to having a single correction for all oxygen compounds.[28] These corrections are obtained by calculating the formation energy of various nontransition metal oxides as

$$\Delta E_{form} = E_{M_xO_y} - xE_M - \frac{y}{2}E_{O_2} \tag{1}$$

where $E_i$ is the total energy calculated in DFT for compound $i$. These calculated formation energies are plotted versus the experimental formation enthalpies at 300 K and 1 atm[29] in Figure 2. We used Li$_2$O, Na$_2$O, MgO, CaO, Al$_2$O$_3$, K$_2$O for
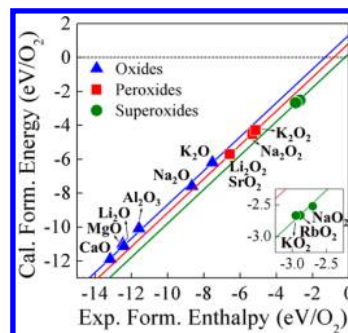


**Figure 2.** Formation energy (in eV/O$_2$) calculated in GGA at 0 K versus the formation enthalpy measured at 300 K and 1 atm for oxides (blue triangles), peroxides (red squares), and superoxides (green circles).[29] The data points corresponding to Li$_2$O$_2$ and SrO$_2$ overlap on this scale. The inset shows zoomed-in formation energies for superoxides. The oxidation energy correction is the $y$-intercept of each line.

oxides, Li$_2$O$_2$, Na$_2$O$_2$, K$_2$O$_2$, SrO$_2$ for peroxides, and NaO$_2$, KO$_2$, RbO$_2$ for superoxides. From this plot, the corrections, $E_{oxd}$, for the calculated oxidation energy are obtained as 1.33, 0.85, and 0.23 eV/O$_2$ for oxides, peroxides, and superoxides, respectively. As no experimental formation enthalpies are known for solid ozonides, no correction energy for O$_3^{-}$ containing solids was obtained. These "corrections", $E_{oxd}$, correct for the error of standard DFT, as well as for the difference in energy between 0 and 300 K.

While it would have been possible to simply shift the calculated formation energy of Na−O compounds to their experimental values, as the formation enthalpies of Na$_2$O, Na$_2$O$_2$, and NaO$_2$ are known, our approach achieves a correction energy that is applicable to a broader range of oxides, as well as to nonbulk states.

To assess the vibrational entropy in the solid states, we performed phonon calculations using the small displacement method within the harmonic approximation. The force constant matrix was constructed using the PHON software[30] based on the Hellman-Feynman forces calculated in GGA when symmetrically distinct atomic displacements were imposed in the structures. The Gibbs free energy is approximated by the Helmholtz free energy as pressure effects on solids can be neglected. The calculated phonon spectrum of $Pa\bar{3}$ NaO$_2$ exhibited imaginary phonon frequencies, indicating that the structure is dynamically unstable (Figure S5 in the SI). Instead we calculated the phonons for the $R\bar{3}m$ NaO$_2$ structure, where all O$_2$ bonds are aligned in one [111] direction (Figure 1f). To represent the rotation of O$_2$ molecules in $Fm\bar{3}m$ NaO$_2$ (disordered form of the $Pa\bar{3}$ structure), we started from the phonon energy and entropy of $R\bar{3}m$ NaO$_2$ and added a fraction of the energy and entropy contributions of a rigid rotor.[31] The fraction was determined so as to reproduce the phase transition temperature between the NaO$_2$ polymorphs, and the equilibrium temperature between Na$_2$O$_2$ and NaO$_2$ at $P_{O_2}$ = 1 atm (see the SI). We also found imaginary frequencies in the

phonon spectrum of $NaO_3$ and will not consider this phase further in this paper. Computational details and results of the phonon computations and approximations can be found in the SI.

The chemical potential of $O_2$ gas as a function of $O_2$ partial pressure and temperature is obtained as follows:

$$\mu_{O_2}(T, P_{O_2}) = E_{O_2}^{total} + \Delta H_{O_2}(T) - TS_{O_2}^{expt}(T)$$
$$+ k_B T(P_{O_2}/P_{O_2}^o) \qquad (2)$$

where $E_{O_2}^{total}$ is the total energy of $O_2$ gas calculated in DFT, $\Delta H_{O_2}$ is the enthalpy difference of $O_2$ gas between 0 K and a given temperature $T$, for which we used the diatomic ideal gas approximation $7/2k_B T$, and $S_{O_2}^{expt}$ is the temperature-dependent entropy of $O_2$ gas at 1 atm as obtained from experiments.[29] The last term is the partial pressure dependence of the entropy of the ideal gas, where $P_{O_2}^o$ is set to 1 atm. We calculate the formation free energies $\Delta G_{form}$ of sodium oxides as a function of $T$ and $P_{O_2}$ by combining the phonon energy of solids, the ($T$, $P_{O_2}$)-dependent chemical potential of oxygen (eq 2), and the oxidation energy correction as in eq S7. The calculated free energies agree well with experimental values (Table 1). Furthermore, our computational results successfully predict the trends in $\Delta G_{form}$ with respect to temperature and the relative stability of Na−O compounds (Figure S8 in the SI).

**Table 1. Calculated Formation Free Energies of Na−O Compounds (Experimental Values[29] in Parentheses) at 0 and 300 K at 1 atm**[a]

| | $\Delta G_{form}$ (eV/Na) | |
|---|---|---|
| compound | 0 K | 300 K |
| $Na_2O$ | −2.17 (−2.14) | −2.00 (−1.96) |
| $Na_2O_2$ | −2.60 (−2.63) | −2.31 (−2.33) |
| $Pnnm$ $NaO_2$ | −2.75 (−2.74) | −2.26 (−) |
| $Fm\overline{3}m$ $NaO_2$ | −2.69 (−) | −2.28 (−2.26) |

[a]Stable phases at each temperature are marked in bold.

Using these free energies, and their $P_{O_2}$ and temperature dependence, we can now calculate the equilibrium $T$−$P_{O_2}$ phase diagram of Na−O compounds (Figure 3). The phase diagram
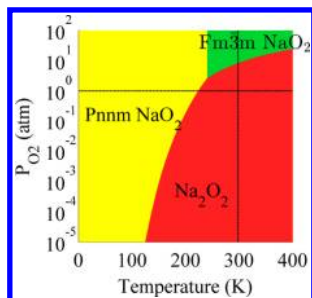


**Figure 3.** Phase diagram of Na−O as function of temperature and $O_2$ partial pressure. Red domain indicates the region where $Na_2O_2$ is stable, yellow domain for $Pnnm$ $NaO_2$, and green domain for $Fm\overline{3}m$ $NaO_2$. The $Pnnm$ $NaO_2$ structure transforms to the $Fm\overline{3}m$ $NaO_2$ at 230−240 K when $P_{O_2}$ = 1 atm, and $Na_2O_2$ is in equilibrium with $Fm\overline{3}m$ $NaO_2$ at 8.5 atm when $T$ = 300 K. The horizontal dashed line denotes $P_{O_2}$ = 1 atm, and the vertical dashed line denotes $T$ = 300 K.

shows that $Na_2O_2$ is the thermodynamically favored phase under standard conditions ($P_{O_2}$ = 1 atm and $T$ = 300 K) and under high temperature or low oxygen pressure. At 300 K, the superoxide $NaO_2$ in the $Fm\overline{3}m$ structure becomes stabilized at a $P_{O_2}$ higher than 8.5 atm, which is much higher than the typical operating conditions of Na−$O_2$ batteries. Therefore, $Na_2O_2$ has been observed as the dominant discharge product in most experiments.[6−9,11] Note that $Na_2O$ is not stable in the $T$ and $P_{O_2}$ range considered, which is consistent with its high experimentally measured formation energy when expressed per Na atom (representing "open $O_2$" conditions (Figure S8 in the SI)).

To understand the relative stability at the nanoscale, where these oxides nucleate, we expand our study to include the surface energies of the relevant polymorphs. We consider the low-index surfaces of $Na_2O_2$ and $Fm\overline{3}m$ $NaO_2$ as they are the competing compounds near room temperature. As $Fm\overline{3}m$ $NaO_2$ has the $O_2$ dimer orientations disordered, we approximate its surface energies by those of ordered $Pa\overline{3}$ $NaO_2$. The surface slab method was used to calculate the surface energies.[4,32] All possible terminations in three low-index surface orientations, {0001}, {1$\overline{1}$00}, and {11$\overline{2}$0} for $Na_2O_2$, and four orientations, {100}, {110}, {111}, and {211} for $Pa\overline{3}$ $NaO_2$ were calculated. The lattice parameters of the surfaces slabs were fixed to the bulk values, while all of the internal parameters were fully relaxed. At the most oxidizing ($O_2$ gas limit) and reducing ($Na_2O$ limit) conditions for $Na_2O_2$, the lowest energy surfaces are either oxygen-rich or stoichiometric, showing shortened surface $O_2$ bonds (1.36−1.51 Å for oxygen-rich terminations and 1.52−1.54 Å for stoichiometric terminations) compared to the $O_2$ bonds lengths in bulk (1.54−1.55 Å). For the surfaces of $NaO_2$, the {100} stoichiometric surface has the lowest energy at both the most oxidizing ($O_2$ gas limit) and reducing ($Na_2O_2$ limit) conditions, and the surface $O_2$ bonds are very slightly extended (1.36 Å) compared to the bulk $O_2$ bonds (1.35 Å). Detailed results of the surface energies and the phase boundary of Na−O compounds can be found in the SI.

From the surface energies, the Wulff shapes and normalized total surface energies per unit volume of particle, $\overline{\gamma}$, can be obtained. The lowest surface energies of $Na_2O_2$ are in the range of 30−45 meV/Å², and the normalized total surface energies $\overline{\gamma}$ are 0.178 and 0.196 eV/Å³ at the most oxidizing amd reducing conditions for $Na_2O_2$, respectively (see the SI for the details on the calculation of $\overline{\gamma}$). The Wulff shape of $Pa\overline{3}$ $NaO_2$ is cubic at both the most oxidizing and reducing conditions. The $NaO_2$ cube is comprised of stoichiometric {100} facets with surface energy of 12 meV/Å², in good agreement with the shape of $NaO_2$ particles seen in SEM pictures by Hartmann et al.[13,14] The normalized total surface energy $\overline{\gamma}$ of $NaO_2$ is 0.070 eV/Å³, much lower than the $Na_2O_2$ surface energies. This lower surface energy is expected to stabilize $NaO_2$ over $Na_2O_2$ at small particle sizes. Although we did not consider possible surface reconstruction in this study, we note that the computed Wulff shape of $NaO_2$ is in good agreement with experimental observations, which indicates that relative surface energies are correct. We therefore do not expect reconstructions to change the fundamental result that the $NaO_2$ surfaces are much lower in energy than the $Na_2O_2$ surfaces.

Figure 4 shows the calculated phase diagram as a function of particle size and oxygen partial pressure. The phase diagram is calculated at the $O_2$ gas limit, but the phase diagrams under
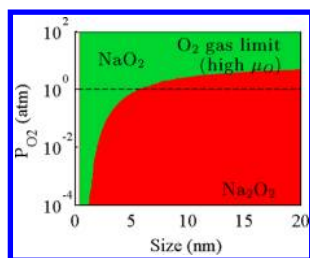
**Figure 4.** Phase diagram of $Na_2O_2$ (red) and $NaO_2$ (green) at 300 K as a function of particle size and $P_{O_2}$ at the $O_2$ gas limit. The particle size is defined as $(V^0)^{1/3}$, where $V^0$ is the total volume of the particle.

other conditions share the same features. Like the bulk phases, $Na_2O_2$ is stable at lower $P_{O_2}$, while $NaO_2$ becomes stabilized at higher $P_{O_2}$. When the particle size decreases, the formation of $NaO_2$ is preferred due to the lower surface energies of $NaO_2$. The particle size at which $Na_2O_2$ becomes more stable than $NaO_2$ at $P_{O_2}$ = 1 atm is ~6 nm at the $O_2$ gas limit. In addition, higher $P_{O_2}$ promotes the stability of bigger $NaO_2$ particles. For example, at $P_{O_2}$ = 4 atm the size of stable $NaO_2$ particle is more than 20 nm.

To further evaluate the initial stage of nucleation during discharge of a Na−$O_2$ battery, we calculated the critical nucleus size $d^*$ and the critical nucleation energy barrier $\Delta G^*$ of $NaO_2$ and $Na_2O_2$ particles (see the SI for details). The critical nucleus size, $(d^*)^3$, represents the particle volume beyond which the particle growth is energetically favorable; $\Delta G^*$ is the free energy required to form this critical nucleus size. We calculated $d^*$ and $\Delta G^*$ as a function of $P_{O_2}$ when the applied potential is 2.1 V versus Na/$Na^+$ corresponding to 0.21 and 0.18 V below the calculated equilibrium potentials for the formation of both $Na_2O_2$ and $NaO_2$, respectively (Table 1). Under this condition, the critical nucleus size for $NaO_2$ is smaller than that for $Na_2O_2$ at $P_{O_2}$ higher than ~0.005 atm (Figure 5a). In addition, the nucleation energy barrier for $Na_2O_2$ is consistently much higher



**Figure 5.** (a, c) The critical nucleus size and (b, d) critical nucleation energy barrier of $Na_2O_2$ and $NaO_2$ particles as a function of $P_{O_2}$ at $\phi$ = 2.1 V vs Na/$Na^+$ (a and b) and as a function of voltage at $P_{O_2}$ = 1 atm (c and d). The applied potential 2.1 V for a and b is 0.21 and 0.18 V lower than the calculated equilibrium potentials of $Na_2O_2$ and $NaO_2$, respectively. These equilibrium potentials of $Na_2O_2$ and $NaO_2$ are marked by vertical lines in c and d.

than that of $NaO_2$ (Figure 5b). Therefore, $NaO_2$ particles are more likely to nucleate because of their smaller critical nucleus size and lower nucleation energy barrier than $Na_2O_2$. The fact that $NaO_2$ nucleates with much lower energy barrier and smaller critical nucleus size than $Na_2O_2$ holds for all discharge potentials, as shown in Figure 5c and d. Furthermore, higher $P_{O_2}$ significantly reduces the critical nucleus size and critical energy barrier for $NaO_2$ particles; the critical nucleus size is less than 1 nm at $P_{O_2}$ = 1 atm (Figure 5a).

We are now in a position to shed light on what controls the formation of either $NaO_2$ or $Na_2O_2$ during discharge of Na−$O_2$ batteries. Considering the formation energy of bulk phases, one can expect that $Na_2O_2$ will be the dominant product at the standard condition (300 K and 1 atm), and $NaO_2$ will form only at extremely high $P_{O_2}$ (>8.5 atm) (Figure 3). However, when the effect of surface energy is taken into account, our computational results reveal that the lower surface energy of $NaO_2$ stabilizes small $NaO_2$ particles over $Na_2O_2$ particles, resulting in the preferred nucleation of $NaO_2$ nanoparticles at any given temperature, $O_2$ pressure, and chemical potential (Figure 4). Given the distinct structure of $NaO_2$ and $Na_2O_2$, and the fact that the energy difference between $NaO_2$ and $Na_2O_2$ is small (20 meV/Na at $d$ = 20 nm, and 30 meV/Na in bulk), these particles may never transform to $Na_2O_2$, remaining metastable. We believe that this may explain the observation of micrometer-sized $NaO_2$ particles by Hartmann et al.[13,14] The formation of $Na_2O_2$ may be favored by poor oxygen transport in electrode caused by, for example, pore clogging. Pore clogging interrupts the $O_2$ supply to nucleation sites and lowers the formation free energy of bulk $Na_2O_2$. For example, when the local $P_{O_2}$ decreases to $10^{-3}$ atm, $Na_2O_2$ particles bigger than 1.5 nm become energetically stable (Figure 4), and when they reach their critical nucleus size, 2.1 nm, there is no obstacle in nucleation of $Na_2O_2$. Thus, to promote $NaO_2$ formation, it is critical to ensure $O_2$ supply by deploying cathode microstructures with high pore-density and/or suitable electrolytes rendering appropriate $O_2$ solubility and diffusion.[33−35]

The thermodynamic stability and formation of the superoxide are significant in controlling the performance of different metal−$O_2$ battery systems. In Li−$O_2$ batteries, the dominant discharge product is $Li_2O_2$, which is difficult to recharge. The overpotential needed to decompose this phase is as high as 1 V, which causes electrolyte decomposition and the formation of byproducts.[36,37] In addition, it is possible that unstable $LiO_2$ is an intermediate state,[26] which creates free superoxide species that attack the electrolyte and carbon support. $NaO_2$ and $KO_2$ are significantly more stable as superoxides. $NaO_2$ formed in a Na−$O_2$ battery can be recharged with small overpotentials (less than 200 mV).[13,14] On the other hand, when $Na_2O_2$ is formed as the discharge product, the discharge and charge overpotentials are high, just as in the Li−$O_2$ system.[6−9] In the K−$O_2$ system, $KO_2$ is even more stable relative to $K_2O_2$ and $K_2O$, and the overpotentials needed to charge it are correspondingly lower at 50 mV.[38] The fact that the formation of the superoxide is a one-electron reduction/oxidation process, as opposed to the two-electron process associated with peroxide, may lead to more facile kinetics, less susceptible to side reactions, and may account for the better kinetics of superoxide charging. These observations indicate that the stability of the superoxide is possibly a key parameter to design viable metal−$O_2$ batteries. Hence, our finding that the formation of superoxide is controlled by its substantially lower nucleation energy at the

nanoscale over peroxide may be particularly important for designing reversible Na−air systems as well as other air batteries.

In summary, we investigated the relative phase stability of $Na_2O_2$ and $NaO_2$ as a function of temperature, $O_2$ partial pressure, and particle size. Our results confirm that in bulk $Na_2O_2$ is stable and $NaO_2$ is metastable at standard conditions. As the superoxide $NaO_2$ has much lower surface energy than the peroxide, it is stabilized when particle size is in the nanometer regime where nucleation takes place. Our results furthermore reveal that the $O_2$ partial pressure is a significant parameter to determine the formation and growth of a particular sodium oxide phase: For higher $O_2$ pressure, the energy barrier to nucleate $NaO_2$ is reduced, and the superoxide remains thermodynamically stable up to larger particle sizes, thereby reducing the possibility that it transforms to the peroxide upon growing.

We expect our findings to direct efforts toward understanding and controlling the formation of desired Na−O compounds in battery operation and furthermore invigorate interest on the potential of Na−$O_2$ batteries.

## ■ ASSOCIATED CONTENT

### Ⓢ Supporting Information

Properties of Na−O compounds, computational details on the phonon calculations, formation free energy formulas, chemical potential ranges, and surface energy calculations. This material is available free of charge via the Internet at http://pubs.acs.org.

## ■ AUTHOR INFORMATION

### Corresponding Author

*E-mail: gceder@mit.edu.

### Present Addresses

Y.M.: Department of Materials Science, Engineering, University of Maryland, College Park, Maryland 20742, United States.
S.P.O.: Department of NanoEngineering, University of California, San Diego, La Jolla, California 92093, United States.

### Notes

The authors declare no competing financial interest.

## ■ ACKNOWLEDGMENTS

## ■ REFERENCES

(1) McHale, J. M.; Auroux, A.; Perrotta, A. J.; Navrotsky, A. *Science* **1997**, *277* (5327), 788−791.

(2) Navrotsky, A.; Mazeina, L.; Majzlan, J. *Science* **2008**, *319* (5870), 1635−1638.

(3) Zhang, H.; Banfield, J. F. *J. Phys. Chem. B* **2000**, *104* (15), 3481−3487.

(4) Ramamoorthy, M.; Vanderbilt, D.; King-Smith, R. D. *Phys. Rev. B* **1994**, *49* (23), 16721−16727.

(5) Navrotsky, A. *ChemPhysChem* **2011**, *12* (12), 2207−2215.

(6) Liu, W.; Sun, Q.; Yang, Y.; Xie, J.-Y.; Fu, Z.-W. *Chem. Commun.* **2013**, *49* (19), 1951−1953.

(7) Li, Y.; Yadegari, H.; Li, X.; Norouzi Banis, M.; Li, R.; Sun, X. *Chem. Commun.* **2013**, *49* (100), 11731−11733.

(8) Sun, Q.; Yang, Y.; Fu, Z.-W. *Electrochem. Commun.* **2012**, *16* (1), 22−25.

(9) Das, S. K.; Xu, S.; Archer, L. A. *Electrochem. Commun.* **2013**, *27*, 59−62.

(10) Peled, E.; Golodnitsky, D.; Mazor, H.; Goor, M.; Avshalomov, S. *J. Power Sources* **2011**, *196* (16), 6835−6840.

(11) Kim, J.; Lim, H.-D.; Gwon, H.; Kang, K. *Phys. Chem. Chem. Phys.* **2013**, *15* (10), 3623−3629.

(12) Jian, Z.; Chen, Y.; Li, F.; Zhang, T.; Liu, C.; Zhou, H. *J. Power Sources* **2014**, *251* (0), 466−469.

(13) Hartmann, P.; Bender, C. L.; Sann, J.; Durr, A. K.; Jansen, M.; Janek, J.; Adelhelm, P. *Phys. Chem. Chem. Phys.* **2013**, *15* (28), 11661−11672.

(14) Hartmann, P.; Bender, C. L.; Vracar, M.; Durr, A. K.; Garsuch, A.; Janek, J.; Adelhelm, P. *Nat. Mater.* **2013**, *12* (3), 228−232.

(15) Wriedt, H. A. *Bull. Alloy Phase Diagrams* **1987**, *8* (3), 234−246.

(16) Sangster, J.; Pelton, A. D. *J. Phys. E* **1992**, *13* (3), 296−299.

(17) Laoire, C. O.; Mukerjee, S.; Abraham, K. M.; Plichta, E. J.; Hendrickson, M. A. *J. Phys. Chem. C* **2009**, *113* (46), 20127−20134.

(18) Laoire, C. O.; Mukerjee, S.; Abraham, K. M.; Plichta, E. J.; Hendrickson, M. A. *J. Phys. Chem. C* **2010**, *114* (19), 9178−9186.

(19) Bryantsev, V. S.; Giordani, V.; Walker, W.; Blanco, M.; Zecevic, S.; Sasaki, K.; Uddin, J.; Addison, D.; Chase, G. V. *J. Phys. Chem. A* **2011**, *115* (44), 12399−12409.

(20) Carter, G. F.; Templeton, D. H. *J. Am. Chem. Soc.* **1953**, *75* (21), 5247−5249.

(21) Templeton, D. H.; Dauben, C. H. *J. Am. Chem. Soc.* **1950**, *72* (5), 2251−2254.

(22) Kresse, G.; Furthmüller, J. *Phys. Rev. B* **1996**, *54* (16), 11169−11186.

(23) Blöchl, P. E. *Phys. Rev. B* **1994**, *50* (24), 17953−17979.

(24) Mo, Y. F.; Ong, S. P.; Ceder, G. *Phys. Rev. B* **2011**, *84* (20), 1−9.

(25) Radin, M. D.; Rodriguez, J. F.; Tian, F.; Siegel, D. J. *J. Am. Chem. Soc.* **2012**, *134* (2), 1093−1103.

(26) Kang, S.; Mo, Y.; Ong, S. P.; Ceder, G. *Chem. Mater.* **2013**, *25* (16), 3328−3336.

(27) Wang, L.; Maxisch, T.; Ceder, G. *Phys. Rev. B* **2006**, *73* (19), 1−6.

(28) Hummelshøj, J. S.; Luntz, A. C.; Nørskov, J. K. *J. Chem. Phys.* **2013**, *138* (3), 034703−034712.

(29) Chase, M. W. *NIST-JANAF thermochemical tables*; American Chemical Society; American Institute of Physics for the National Institute of Standards and Technology: Washington, DC, 1998.

(30) Alfe, D. *Comput. Phys. Commun.* **2009**, *180* (12), 2622−2633.

(31) McQuarrie, D. A. *Statistical Mechanics*; University Science Books: South Orange, NJ, 2000.

(32) Reuter, K.; Scheffler, M. *Phys. Rev. B* **2001**, *65* (3), 035406.

(33) Song, M.-K.; Park, S.; Alamgir, F. M.; Cho, J.; Liu, M. *Mater. Sci. Eng. R* **2011**, *72* (11), 203−252.

(34) Xiao, J.; Mei, D.; Li, X.; Xu, W.; Wang, D.; Graff, G. L.; Bennett, W. D.; Nie, Z.; Saraf, L. V.; Aksay, I. A.; Liu, J.; Zhang, J.-G. *Nano Lett.* **2011**, *11* (11), 5071−5078.

(35) Read, J. *J. Electrochem. Soc.* **2002**, *149* (9), A1190−A1195.

(36) Christensen, J.; Albertus, P.; Sanchez-Carrera, R. S.; Lohmann, T.; Kozinsky, B.; Liedtke, R.; Ahmed, J.; Kojic, A. *J. Electrochem. Soc.* **2012**, *159* (2), R1−R30.

(37) Lee, J.-S.; Tai Kim, S.; Cao, R.; Choi, N.-S.; Liu, M.; Lee, K. T.; Cho, J. *Adv. Energy Mater.* **2011**, *1* (1), 34−50.

(38) Ren, X.; Wu, Y. *J. Am. Chem. Soc.* **2013**, *135* (8), 2923−2926.